Zierenberg, R.A., Fouquet, Y., Miller, D.J., and Normark, W.R. (Eds.),
Proceedings of the Ocean Drilling Program, Scientific Results Volume 169

1. Data Report: Trace Element Geochemistry of I^-, Br^-, F^-, HPO_4^{2-}, Ba^{2+}, and Mn^{2+} in Pore Waters of Escanaba Trough, Sites 1037 and 1038[1]

Joris M. Gieskes,[2] Chris Mahn,[2] and Barni Schnetzger[3]

INTRODUCTION

Data were presented to compare pore fluids from Sites 1037 and 1038 in the Escanaba Trough, Gorda Ridge. Site 1037 constitutes the reference site, and Site 1038 is the hydrothermally affected site. The program was undertaken for two purposes: (1) to make a detailed analysis of the halide chemistry of these two sites, with the specific aim of discerning any potential differences in the generation of dissolved halides as a result of sediment diagenesis in these drill sites and (2) to investigate the geochemistry of Ba^{2+} and Mn^{2+} at these two sites to discover potential hydrothermal effects reflected in the concentration-depth distributions of these elements.

METHODS

Halides

Analyses for the dissolved halides I^-, Br^-, and F^- were carried out by means of colorimetric methods described in the Ocean Drilling Program (ODP) Technical Note 15 (**http://www-odp.tamu.edu/publications/tnotes/tn15/f_chem1.htm**) (Gieskes et al., 1991). Accuracies are ~5% for iodide and bromide.

[1]Gieskes, J.M., Mahn, C., and Schnetzger, B., 2000. Data report: Trace element geochemistry of I^-, Br^-, F^-, HPO_4^{2-}, Ba^{2+}, and Mn^{2+} in pore waters of Escanaba Trough, Sites 1037 and 1038. *In* Zierenberg, R.A., Fouquet, Y., Miller, D.J., and Normark, W.R. (Eds.), *Proc. ODP, Sci. Results,* 169, 1–16 [Online]. Available from World Wide Web: <http://www-odp.tamu.edu/publications/169_SR/VOLUME/CHAPTERS/SR169_01.PDF>. [Cited YYYY-MM-DD]
[2]Scripps Institution of Oceanography, La Jolla CA 92093-0215, USA. Correspondence author: **jgieskes@ucsd.edu**
[3]Institut für Chemie und Biologie des Meeres, Carl von Ossietzky University of Oldenburg, 26111 Oldenburg, Federal Republic of Germany.

Date of initial receipt: 22 February 1999
Date of acceptance: 18 August 1999
Date of publication: 15 April 2000
Ms 169SR-103

Fluoride determinations utilized the method by Greenhalgh and Riley (1961). A modification of their original method allows the use of 500-µL samples instead of 15-cm^3 samples. The scaled-down method used only 500 µL of sample diluted with 1 cm^3 of deionized water. Because diluting the sample with deionized water was necessary to ensure sufficient liquid for analysis, samples had higher pH conditions than the optimal range 4.45–4.85 for fluoride determinations (Greenhalgh and Riley, 1961). To readjust the pH values of the samples so that they were within this range, 27 µL of 6 M acetic acid was added. Finally, 800 µL of the mixed lanthanum-alizarin reagent was then added. After all the reagents were added to the sample, the fluoride concentration was determined 30 min later on a spectrophotometer at 622 nm.

The fluoride standards were created in the following manner. A stock solution of NaF was made by dissolving sodium fluoride in deionized water and a small volume of 0.1 M sodium hydroxide. Synthetic seawater was then prepared (558 mM sodium chloride and 3 mM sodium bicarbonate). Appropriate volumes of the stock solution were diluted to 100 mL with the synthetic seawater to create standards of 20, 40, and 60 µM NaF. A blank was also used that was composed only of synthetic seawater. These standards were run using the same method listed above, and sample concentrations were determined from the standard curve. Changes in the concentrations of magnesium and calcium can, in principle, affect the data. However, overall changes will not be affected by this.The accuracy of the fluoride method is ±5 µM.

Phosphate

Dissolved phosphate was analyzed by means of the colorimetric technique described in Gieskes et al. (1991) (**http://www-odp.tamu.edu/publications/tnotes/tn15/f_chem1.htm**). Accuracies are low because only small quantities of fluids were available for analysis (±2 µM).

Barium and Manganese

Concentrations of Ba^{2+} and Mn^{2+} were determined using the ICP-MS at the University of Oldenburg. All data obtained are presented in Tables T1 and T2 of this report. Wherever appropriate, graphic representations are used.

T1. Interstitial water chemistry, Hole 1037B, p. 14.

T2. Interstitial water chemistry, Site 1038, p. 15.

DATA PRESENTATION

Halides

Hydrothermal fluids from vents associated with the hydrothermal field at Site 1038 in the Escanaba Trough are characterized by the following halide concentrations (Campbell et al., 1994):

$$Cl = 670\ mM;\ I = 99\ \mu M;\ Br = 1179\ \mu M;\ with\ Br/Cl = 1.76 \cdot 10^{-3}.$$

These data are typical for sedimented ridge hydrothermal fluids (Campbell and Edmond, 1989; Magenheim and Gieskes, 1992; You et al., 1994) in that fluids with elevated chloride concentrations and relatively high iodide and bromide concentrations commonly reflect interactions between hydrothermal fluids and organic-carbon-rich sediments.

Preliminary data on the distribution of the halide concentrations obtained in Sites 1037 and 1038 are presented in Gieskes et al. (1998). These results are discussed in greater detail elsewhere (J. Gieskes et al., unpubl. data). The principal results for both sites are presented as concentration vs. depth distributions of Cl^-, I^-, and Br^- in Hole 1037B (Escanaba reference site) in Figure **F1**. Figures **F2** and **F3** present the data obtained at Site 1038, the hydrothermal site in Escanaba Trough.

The predominant features evident in the compositional profiles in Hole 1037B are the peaks in halide concentrations at ~400 meters below seafloor (mbsf). A recent hydrothermal event has left its imprint on the pore fluid chemistry. Perhaps this hydrothermal event may have affected the pore fluid composition at the base of Hole 1037B (Fouquet, Zierenberg, Miller, et al., 1998). This hydrothermal event may have caused minor boiling or phase separation, thus creating a layer of low chloride content.

The concentration-depth profiles of Cl^-, I^-, and Br^- in the upper sections of Site 1038 (Holes 1038B through 1038H; Fig. **F2**) show complex distributions. For reference, the Cl^-, I^-, and Br^- concentrations, as well as the Br/Cl ratios for seawater and the vent fluids, are presented as vertical dashed lines. Many of the chloride concentrations are above those of seawater, but for Hole 1038H they also indicate values below those of seawater. The low concentrations are in sandy horizons, and these low concentrations have been interpreted in terms of lateral advection of a low chloride end-member of a phase-separated hydrothermal fluid (Fouquet, Zierenberg, Miller, et al., 1998). In Hole 1038C, Hole 1038D, and particularly in Holes 1038F and 1038G, as well as the deeper part of Hole 1038H, elevated concentrations are commonly above those of the previously sampled vent fluids. In Hole 1038B, there is some evidence for higher chloride fluids at depths shallower than 35 mbsf, but, below this depth horizon, seawater values indicate chloride value penetration of recent seawater in a recharge zone situation (cf. Fouquet, Zierenberg, Miller, et al., 1998). Both elevated-chloride and low-chloride fluids are in samples from Hole 1038H, indicating lateral movements of both types of hydrothermal fluids. Iodide concentrations indicate the production of iodide in all hydrothermal fluids, with particularly high values in Holes 1038F and 1038G. Bromide concentrations also are elevated in the hydrothermally affected sediments, with Br/Cl ratios agreeing with the vent fluids in only a few cases, the ratios usually being higher than the vent values.

The broad minimum in the chloride concentrations in Hole 1038I (Fig. **F3**) has been explained in terms of an intrusion of a phase-separated fluid through permeable sand layers (see Fig. **F2**: Holes 1038B and 1038H), characteristic of these horizons (Fouquet, Zierenberg, Miller, et al., 1998). The data for chloride indicate a broad minimum centered around the sill in Hole 1038I. Just below the sill, however, a clear maximum occurs in the chloride profile. This maximum may be associated with the sill intrusion, either as a result of lateral advection of a high-chloride fluid or as a result of dehydration reactions associated with the sill intrusion. Below a depth of ~350 mbsf, chloride concentrations again decrease, possibly associated with a low-chloride zone below the sill at the base of Hole 1038I. Concentrations of iodide change with depth. Maxima are associated with the zones of "normal" chloride concentrations, which suggests that much of the iodide increases result from diagenesis of organic matter in the zones least affected by hydrothermal fluids. The low iodides around the sill intrusion are probably associated with the low chloride fluids (see also Fig. **F2**: Hole 1038H).

F1. Chloride, iodide, and bromide in pore fluids of Hole 1037B, p. 7.

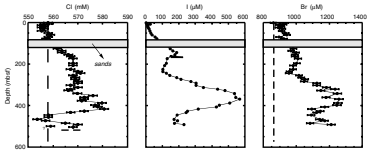

F2. Chloride, iodide, bromide, and Br/Cl ratio in pore fluids of Holes 1038B–1038H, p. 8.

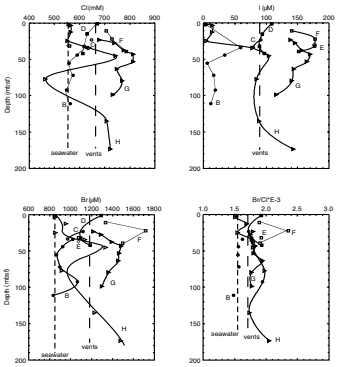

F3. Chloride, iodide, bromide, and Br/Cl ratios in pore fluids of Hole 1038I, p. 9.

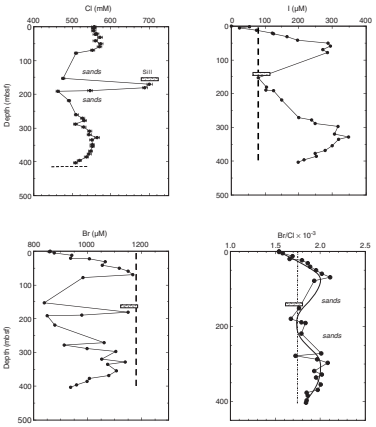

Bromide concentrations follow those of chloride, but it is evident from the Br/Cl ratios that, in the hydrothermally affected zone around the sill intrusion, the Br/Cl ratios are close to those of the vent fluids.

The distribution of fluoride is presented in Figure F4. Holes 1038G and 1038H contain a substantial component of hydrothermally influenced fluid (Gieskes et al., 1998; James and Palmer, 1998), and, in both cases, relatively high F^- concentrations are observed. The increase in fluoride toward the bottom of Hole 1037B suggests hydrothermal alteration of sediments just above the basalt/sediment interface.

Phosphate concentrations were measured only in the reference Hole 1037B. The data are presented in Figure F5 and show substantial variations in the phosphate concentrations mostly in the sediments above the sand layers. There is a rough correlation with the concentrations of fluoride, presumably as a result of fluorophosphate precipitation reactions. Below the sand layers, phosphate concentrations are generally near zero, especially below ~250 mbsf (i.e., coincident with the near-zero concentrations between 250 and 400 mbsf).

Barium and Manganese

A potential problem with the Ba data results from possible sampling artifacts from the addition of seawater sulfate during sample retrieval. The addition of seawater sulfate would cause the precipitation of $BaSO_4$. This artifact plagues the data, especially in Hole 1037B, where zero sulfate concentrations would be expected below the sandy horizon. Figure F6 demonstrates this problem. Some samples have as much as 5 mM of SO_4^{2-}, but most samples are below 2 mM SO_4^{2-}, that is, a contamination of 7% or less. Only a few samples had zero sulfate concentrations (Fig. F6: large solid circles), but these samples allow us to propose the contours of the "actual" Ba^{2+} distribution. Although we have no knowledge of the true magnitude of the Ba^{2+} concentration at ~325 mbsf, there remains little doubt that concentrations well in excess of 300 µM are in this depth horizon.

As indicated above, the data on dissolved barium are too scattered to indicate significant regeneration of this component, except perhaps at ~325 mbsf in Hole 1037B, where the data indicate a broad maximum in Ba^{2+}. The concentrations in the region of the sill in Hole 1038I also indicate potential regeneration of Ba^{2+} in that zone, but this is speculative.

Concentrations of dissolved manganese in Hole 1037B show regeneration of Mn^{2+} in the upper sediment layers and a broad maximum around the depth horizon of ~425 mbsf (Fig. F7). At Site 1038, Mn^{2+} shows increased concentrations near the sediment/water interface, as well as evidence for Mn^{2+} mobilization associated with the hydrothermal fluids associated with high chlorides in Hole 1038G. Not enough sample was available for the sediments from Hole 1038I in the vicinity of the sill at ~160 mbsf. There is evidence, however, that elevated Mn^{2+} may occur in this zone. Below 200 mbsf in Hole 1038I, dissolved Mn^{2+} indicates a maximum at ~360 mbsf, a sediment horizon that appears equivalent to the horizon of elevated Mn^{2+} in the deeper part of Hole 1037B.

F4. Fluoride concentrations in Sites 1037 and 1038, p. 10.

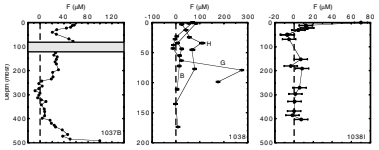

F5. Phosphate concentrations in Hole 1037B, p. 11.

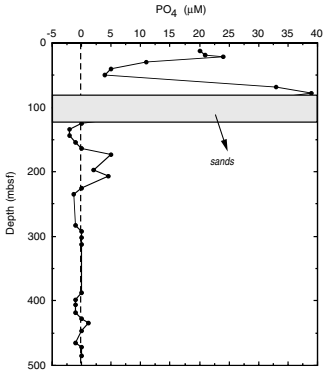

F6. Sulfate and barium concentrations in pore fluids of Hole 1037B, p. 12.

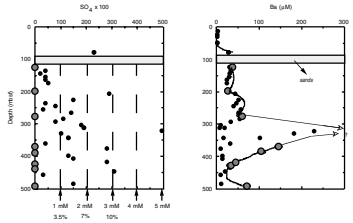

F7. Manganese and barium concentrations from Sites 1037 and 1038, p. 13.

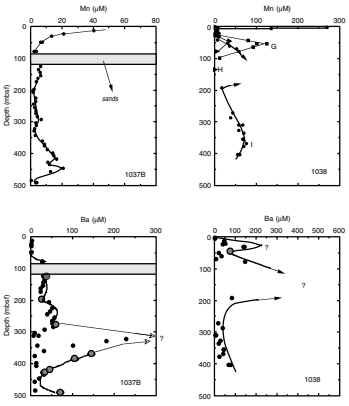

ACKNOWLEDGMENTS

This work was supported by JOI-USSAC postcruise funds. Joris Gieskes thanks Hans Brumsack of the Institut für Chemie und Biologie des Meeres, Carl von Ossietzky University of Oldenburg, for hosting him on a special fellowship of the Hanse Institute of Bremen/Oldenburg. Geoffrey Wheat and Robert Zierenberg reviewed the manuscript critically, improving it greatly.

REFERENCES

Campbell, A.C., and Edmond, J.M., 1989. Halide systematics of submarine hydrothermal vents. *Nature,* 342:168–170.

Campbell, A.C., German, C.R., Palmer, M.R., Gamo, T., and Edmond, J.M., 1994. Chemistry of hydrothermal fluids from the Escanaba Trough, Gorda Ridge. *In* Morton, J.L., Zierenberg, R.A., Reiss, C.A. (Eds.), *Geologic, hydrothermal, and biologic studies at Escanaba Trough, Gorda Ridge, offshore Northern California*. U.S. Geol. Surv. Bull., 2022:201–221.

Fouquet, Y., Zierenberg, R.A., Miller, D.J., et al., 1998. *Proc. ODP, Init. Repts.,* 169: College Station, TX (Ocean Drilling Program).

Gieskes, J.M., Gamo, T., and Brumsack, H., 1991. Chemical methods for interstitial water analysis aboard *JOIDES Resolution. ODP Tech. Note,* 15.

Gieskes, J.M., Mahn, C., James, R., and Ishibashi, J., 1998. Halide systematics in sedimentary hydrothermal systems, Escanaba Trough, ODP Leg 169. *In* Arehart, G.B., and Hulston, J.R. (Eds.), *Water-Rock Interaction:* Rotterdam (Balkema), 723–726.

Greenhalgh, R., and Riley, J.P., 1961. The determination of fluoride in natural waters, with particular reference to seawater. *Anal. Chim. Acta,* 25:179–188.

James, R.H., and Palmer, M.R., 1998. Alkali element and B geochemistry of sedimented hydrothermal systems *In* Arehart, G.B., and Hulston, J.R. (Eds.), *Water-Rock Interaction:* Rotterdam (Balkema), 739–743.

Magenheim, A.J., and Gieskes, J.M., 1992. Hydrothermal discharge and alteration in near-surface sediments from the Guaymas Basin, Gulf of California. *Geochim. Cosmochim. Acta,* 56:2329–2338.

You, C.-F., Butterfield, D.A., Spivack, A.J., Gieskes, J.M., Gamo, T., and Campbell, A.J., 1994. Boron and halide systematics in submarine hydrothermal systems: effects of phase separation and sedimentary contributions. *Earth. Planet. Sci. Lett.,* 123:227–238.

Figure F1. Chloride, iodide, and bromide in pore fluids of Hole 1037B.

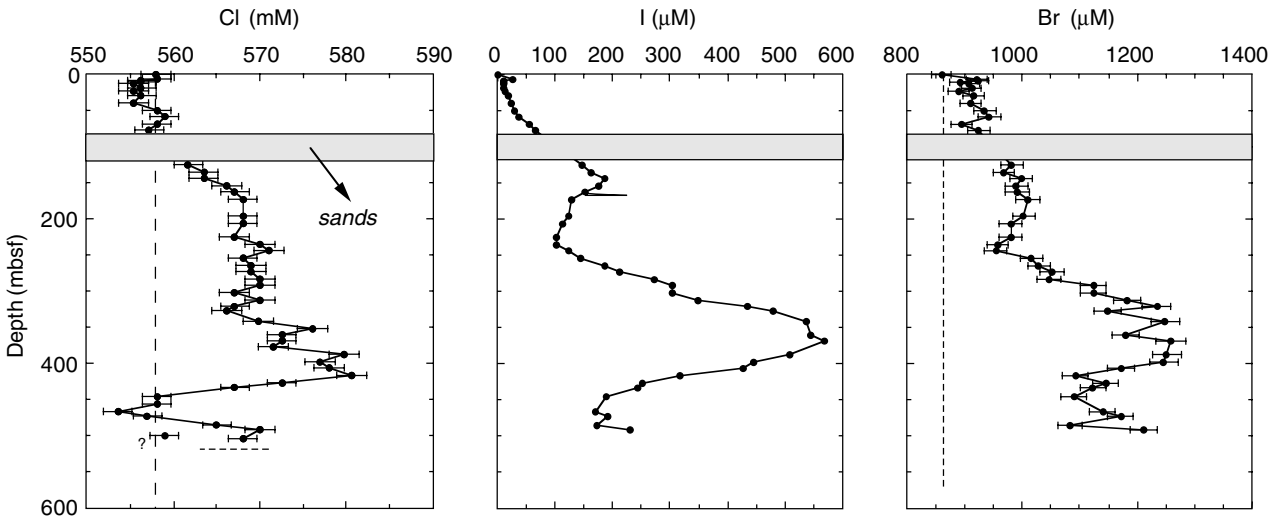

Figure F2. Chloride, iodide, bromide, and Br/Cl ratio in pore fluids of Holes 1038B–1038H. Dashed lines represent seawater and vent fluid concentrations/ratios. Letters correlate with hole designations from Site 1038.

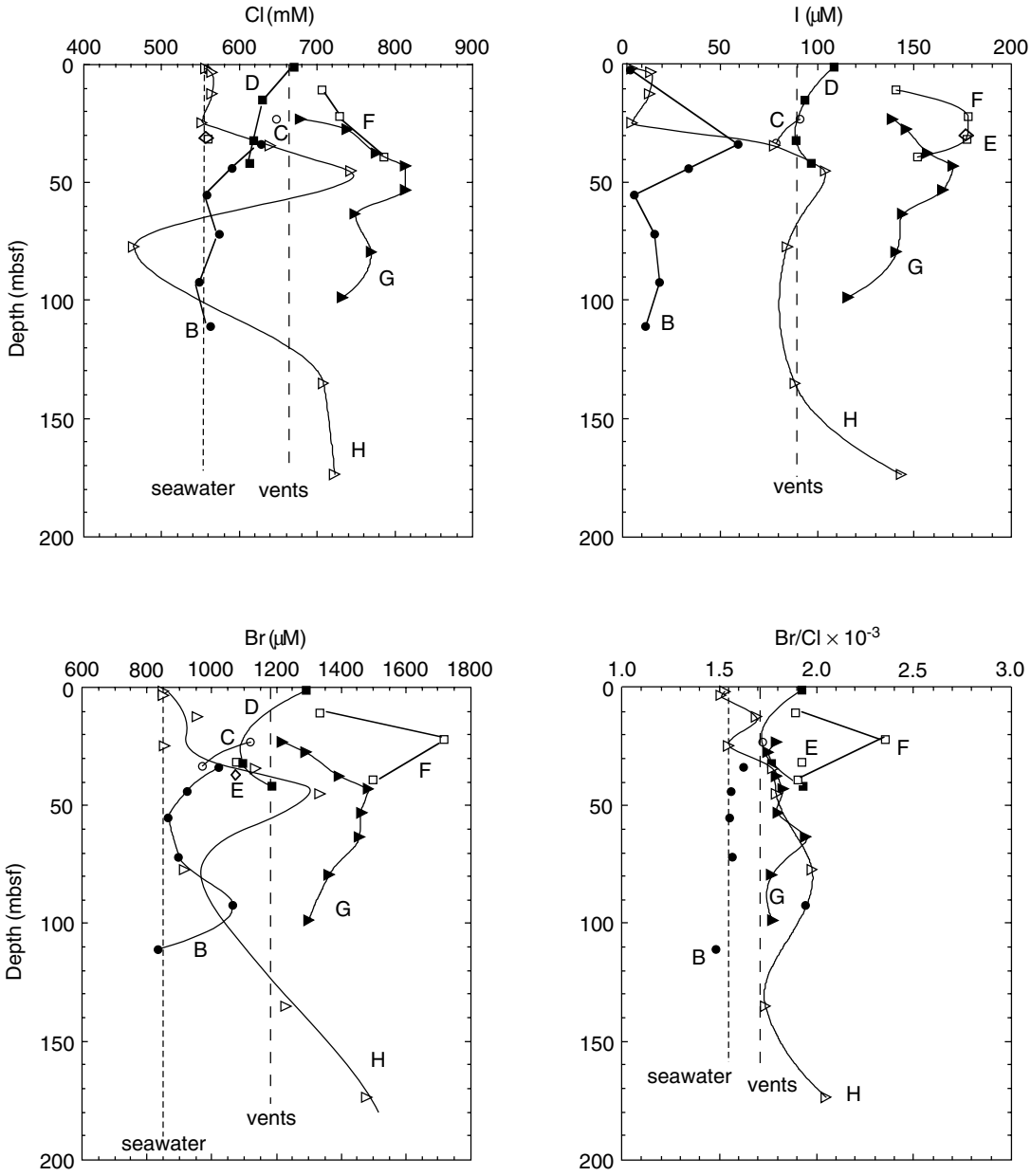

Figure F3. Chloride, iodide, bromide, and Br/Cl ratios in pore fluids of Hole 1038I. Dashed lines represent vent fluid compositions.

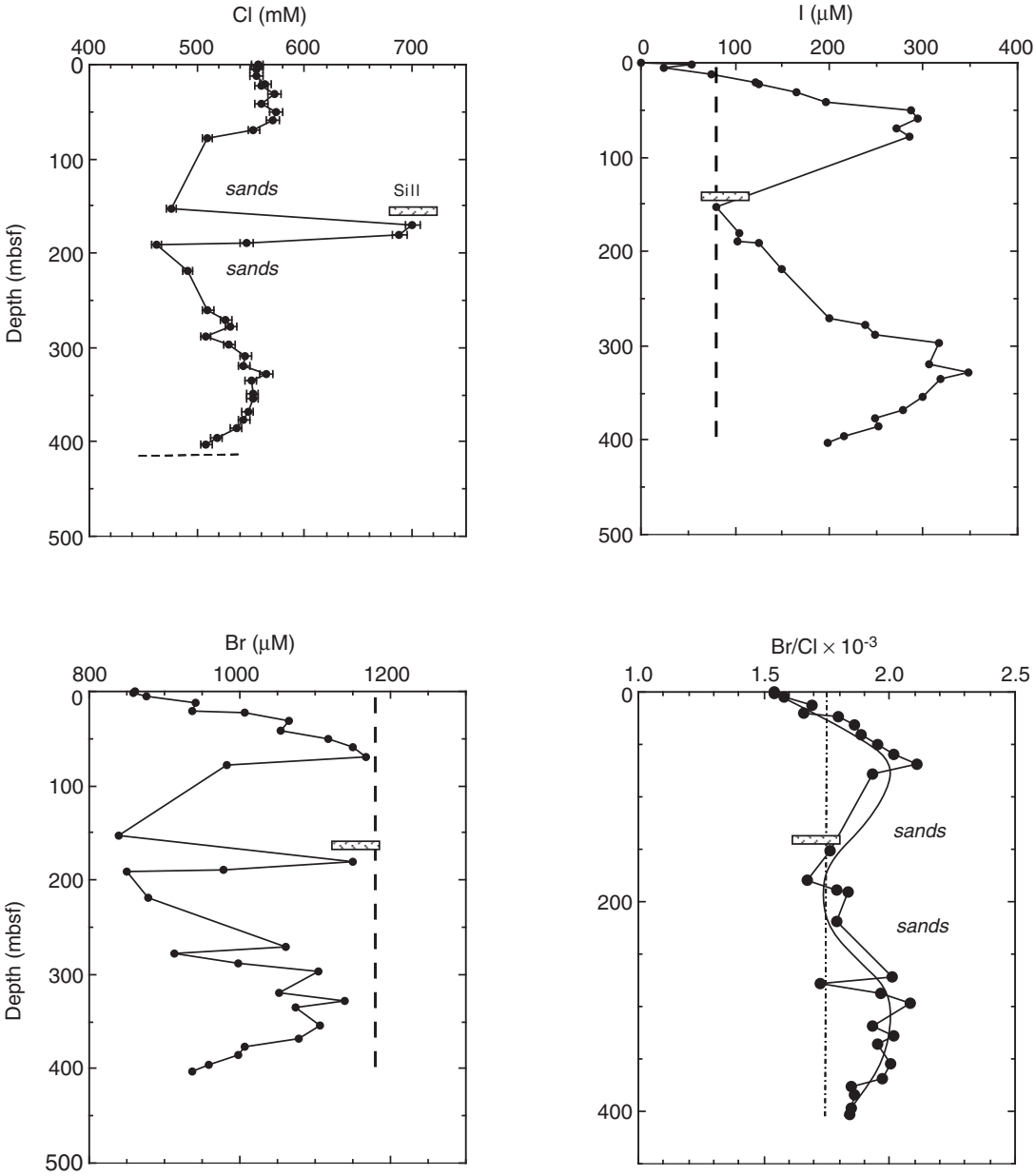

Figure F4. Fluoride concentrations in Sites 1037 and 1038.

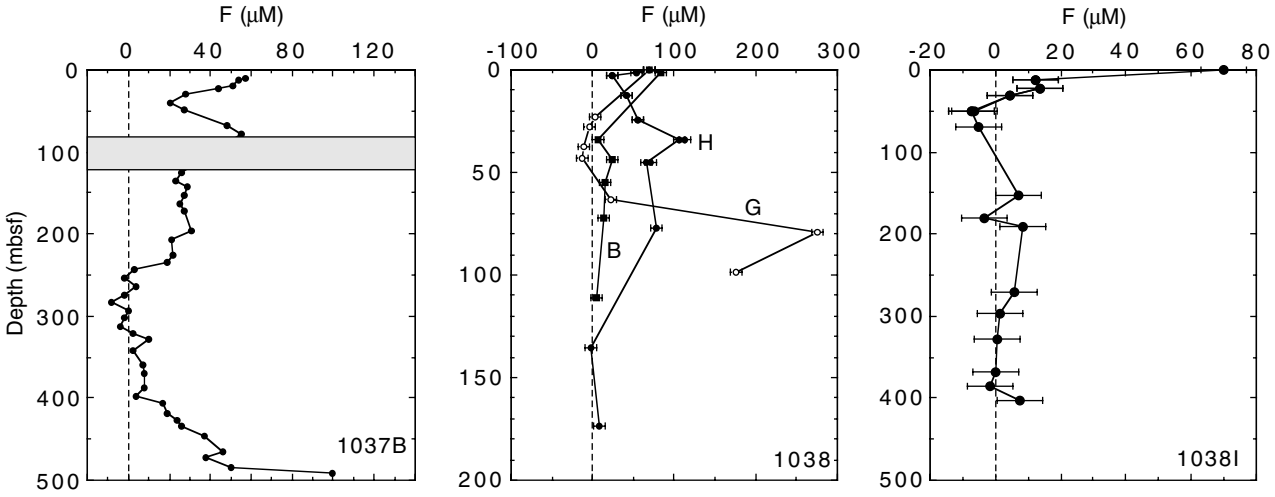

Figure F5. Phosphate concentrations in Hole 1037B.

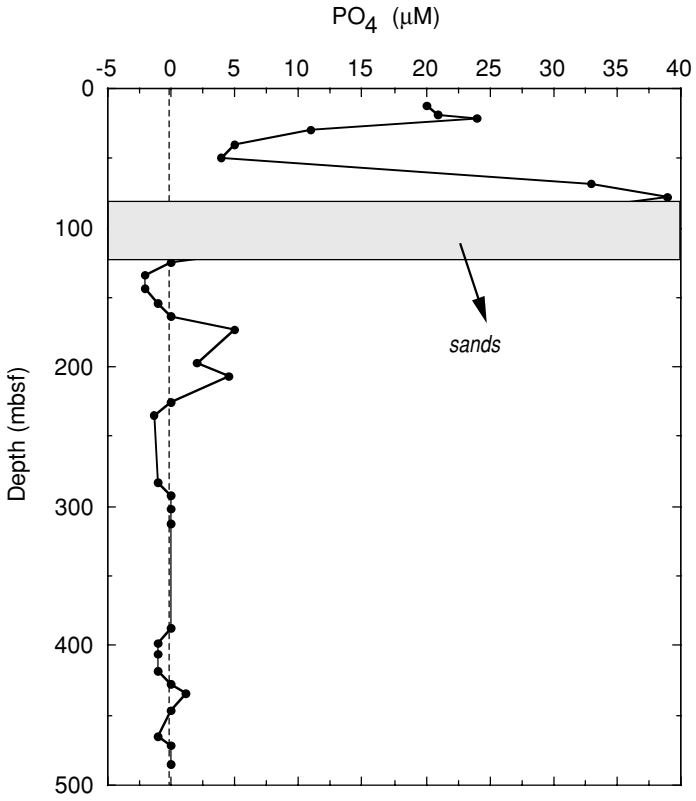

Figure F6. Sulfate and barium concentrations in pore fluids of Hole 1037B. Enlarged circles represent zero sulfate samples with "best" estimates of the Ba^{2+} concentrations. In the SO_4^{2+} plot, note estimates of percentage contamination with seawater.

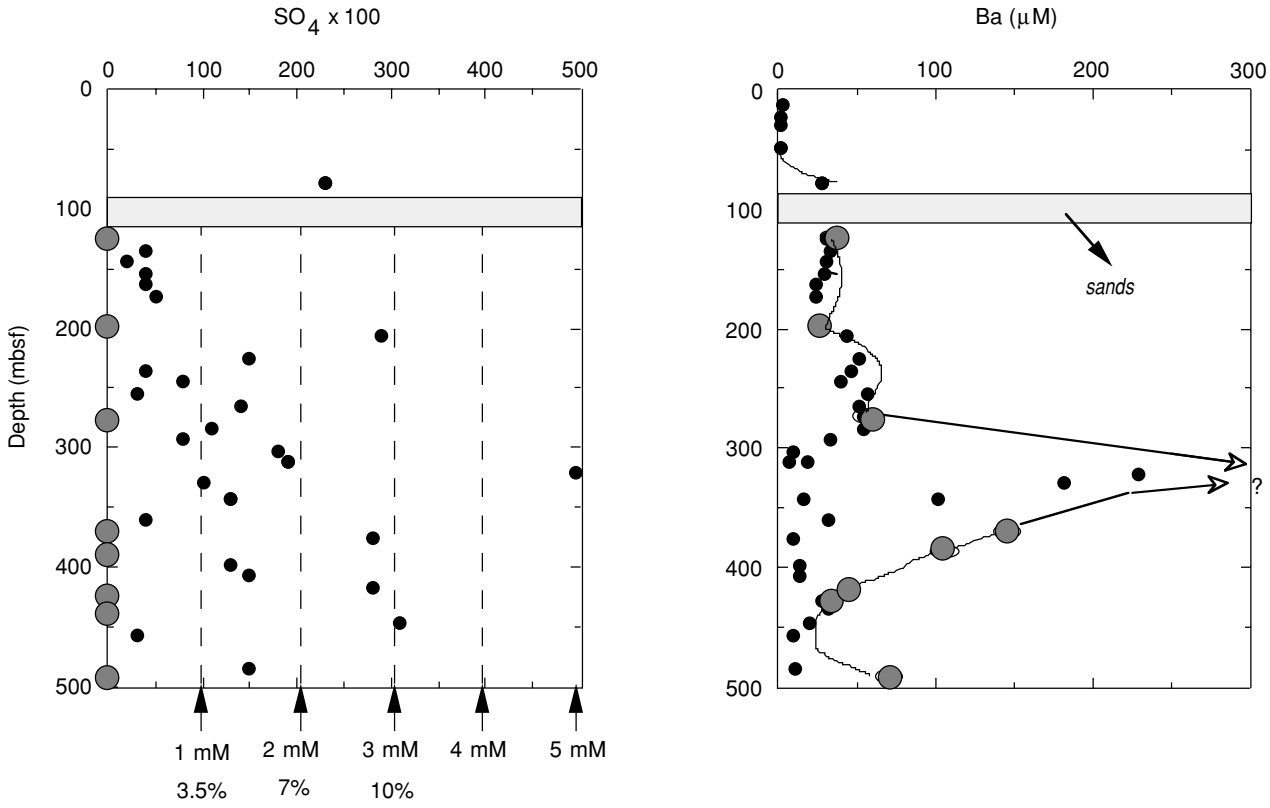

Figure F7. Manganese and barium concentrations from Sites 1037 and 1038.

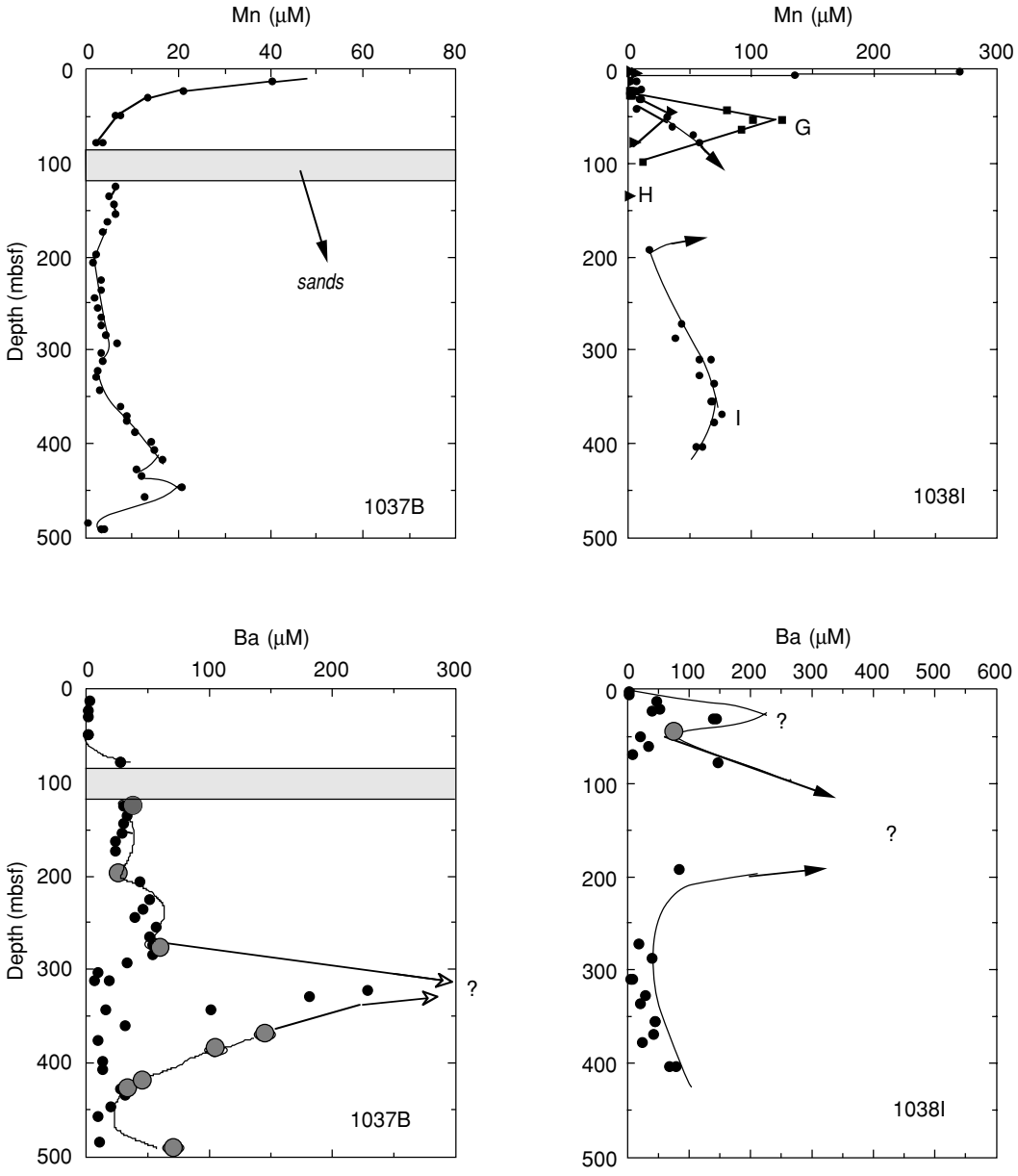

Table T1. Interstitial water chemistry, Hole 1037B.

Core, section, interval (cm)	Depth (mbsf)	Ba (μM)	Mn (μM)	I (μM)	Br (μM)	F (μM)	Cl (mM)	PO_4 (μM)
169-1037B-								
2H-2,140-150	9.6			11	891	57	556	
2H-4, 140-150	12.6	2	40	11	909	54	555	20
3H-2, 140-150	19.1			11	911	51	556	21
3H-4, 140-150	22.1	1	21	13	889	44	555	24
4H-3, 140-150	30.1	1	13	20	915	28	556	11
5H-3, 140-150	39.6			24	909	20	555	5
6H-3, 140-150	49.1	1	7	29	935	27	558	4
7H-2, 140-150	68.1			56	894	48	559	33
9H-3, 140-150	77.6	28	3	66	924	55	557	39
14H-3, 140-150	125.0	31	6	148	982	26	562	0
15H-3, 140-150	134.6	33	5	163	968	23	564	–2
16H-3, 140-150	143.1	30	6	186	998	29	564	–2
17H-3, 140-150	153.6	28	6	175	990	27	566	–1
18H-3, 140-150	163.1	23	5	153	991	25	567	0
20X-3, 140-150	172.6	23	3	128	1009	27	568	5
22X-2, 140-150	196.7	24	3	124	1003	31	568	2
23X-3, 140-150	206.3	43	1	114	979	21	568	5
25X-3, 140-150	225.5	51	3	102	981	22	567	0
26X-3, 140-150	235.1	47	3	104	957	19	570	–1.3
27X-2, 140-150	243.2	39	2	124	954	3	571	
28X-3, 140-150	254.3	57	3	145	1016	–2	568	
29X-3, 140-150	264.0	51	3	185	1029	4	569	
30X-3, 140-150	273.5	53	3	212	1050	–2	569	
31X-3, 140-150	283.0	54	4	273	1046	–8	570	–1
32X-3, 140-150	292.6	33	7	303	1124	0	570	0
33X-3, 140-150	302.2	9	3	304	1124	–2	567	0
34X-3, 140-150	311.8	19	3	349	1181	–4	570	0
35X-4, 140-150	321.4	229	2	434	1234	2	567	
36X-1, 140-150	328.0	181	2	479	1148	10	566	
37X-4, 140-150	342.1	102	3	537	1248	2	570	
39X-3, 140-150	360.0	31	7	544	1178	7	573	
40X-3, 140-150	369.5	142	9	570	1259	8	573	
41X-4, 140-150	376.2	9	9					
42X-2, 140-150	387.3	104	10	508	1251	8	580	0
43x-3, 140-150	398.4	13	14	444	1246	4	577	–1
44X-2, 140-150	406.6	14	15	428	1173	17	578	–1
45X-3, 140-150	417.7	45	17	317	1092	19	581	–1
46X-3, 140-150	427.3	27	12	252	1145	24	573	0
47X-1, 140-150	433.9	31	12	244	1123	26	567	1
48X-3, 140-150	446.5	20	21	188	1089	37	558	0
49X-3, 140-150	456.1	10	12					
50X-3, 140-150	465.8			170	1140	46	554	–1
51X-1, 140-150	472.4			191	1171	38	557	0
52X-3, 140-150	485.0	11	0	172	1083	50	565	0
53X-1, 140-150	491.6	70	4	231	1211	100	570	

Table T2. Interstitial water chemistry, Site 1038. (See table note. Continued on next page.)

Core, section, interval (cm)	Depth (mbsf)	Ba (µM)	Mn (µM)	I (µM)	Br (µM)	F (µM)	Cl (mM)
169-1038B-							
1R-1, 140-150	2.0						
5R-1, 19-29	34.0			4	616	83.00	628.00
6R-1, 22-31	43.8			59	1021	7.00	591.00
7R-2, 51-56	55.2			34	923	23.00	558.00
8R-CC, 3-15	72.0			6	866	15.00	574.00
11R-1, 3-8	92.0			16	899	13.00	548.00
13R-1, 60-70	111.2			19	1065		554.00
				12	835	4.50	563.00
169-1038C-							
3R-1, 85-95	23.0			91	1118		648.00
4R-1,51-61*	33.0			79	971		573.00
169-1038D-							
1R-1, 136-146	1.0			109	1292		671.00
2R-1, 58-61	15.0			94			629.00
3R-1, 35-40	32.0			89	1095		618.00
4R-CC, 5-10	42.0			97	1185		614.00
169-1038E, 1038F-							
F2R-1, 100-110	10.6			141	1335		706.00
F3R-2, 140-150	22.1			178	1716		729.00
E4R-2, 45-55	31.4			177	1076		559.00
F4R-CC, 0-8	39.0			152	1498		786.00
169-1038G-							
3H-2, 140-150	23.0	42	2	139	1217	3.20	679.00
3H-5, 140-150	27.5	190	3	146	1293	–4.00	739.00
4H-5, 38-46	37.5			157	1395	–12.00	776.00
5H-2, 140-150	43.0	87	80	170	1484	–13.00	813.00
6H-1, 140-150	53.0	22	125	165	1462		813.00
7X-2, 140-15*	63.5	11	93	144	1457	22.00	748.00
8X-CC, 3-9	79.5			141	1362	276.00	769.00
10X-CC, 26-34	98.8	16	12	116	1300	176.00	732.00
169-1038H-							
1X-1, 140-150	1.5	2	3	4	850	54.00	556.00
1X-2, 140-150	3.0	1	6	14	852	24.00	564.00
2X-1, 140-150	12.4	1	4	14	956	42.00	565.00
3X-2, 140-150	24.5	3	6	5	853	56.00	551.00
4X-3, 140-150	34.3			78	1137	105.00	640.00
5X-4, 140-150	45.1	92	36	104	1333	67.00	744.00
8X-CC, 19-28	77.0	13	6	85	917	78.00	464.00
14X-CC, 29-35	135.1	38	2	89	1230	–2.00	708.00
16X-CC, 17-21	173.5			143	1478	8.00	722.00
169-1038I-							
1X-1, 140-150	1.5	2	269				
1X-3, 140-150	4.5	2	135	53	858		555.00
2X-2,0140-150	12.3	47	7	24	876		555.00
3H-2, 14-150	20.3	52	11	75	940	12.00	564.00
3H-4, 140-150	23.3	38	7	121	936		560.00
4H-3, 140-150	31.3	140	9	125	1007	14.00	572.00
5H-3, 140-150	40.8	79	6	165	1065	4.00	560.00
6H-3, 140-150	50.3	20	32	196	1055		573.00
7H3, 140-150	59.8	34	35	224	1117	–6.50	571.00
8X-3, 140-150	69.2	7	52	224	1150		553.00
9X-2, 140-150	77.4	147	58	224	1168	–5.00	509.00
17X-1, 119-129	152.0			224	983		476.00
18X-CC, 17-24	170.3			81	839	7.00	700.00
19X-CC, 23-28	180.0						688.00
20X-CC, 29-34	189.6			104	1150	–3.00	546.00
21X--1, 140-150	191.2	83	17	102	977		462.00
23X-CC, 24-29	218.5			126	849	8.00	491.00
28X-2, 140-150	260.0			149	879		510.00
29X-3, 140-150	271.2	18	43				527.00
30X-1, 140-150	278.0			200	1061	6.00	531.00
31X-2, 140-150	287.6	39	39	238	914		508.00
32X-1, 140-150	297.2			249	998		530.00
33X-3, 140-150	309.8	6	63	317	1105	1.00	545.00

Table T2 (continued).

Core, section, interval (cm)	Depth (mbsf)	Ba (μM)	Mn (μM)	I (μM)	Br (μM)	F (μM)	Cl (mM)
34X-3, 140-150	319.4						544.00
35X-2, 140-150	327.5	28	57	306	1052		564.00
36X-2, 140-150	335.6	20	69	348	1139	0.56	550.00
37X-4, 140-150	349.7			318	1074		552.00
38X-1, 140-150	354.8	45	68				552.00
39X-4, 140-150	368.9	43	77	300	1106		547.00
40X-3, 140-150	377.0	24	70	279	1079	0.00	544.00
41X-1, 140-150	385.1			248	1007		536.00
42X-3, 140-150	396.3			252	997		518.00
43X-1, 90-100	402.4	73	58	198	938	7.40	509.00

Note: * = possible contamination.